

# On CNN Boundary Conditions in Turing Pattern Formation

Liviu Goras<sup>1</sup> and Tiberiu Teodorescu<sup>2</sup>

<sup>1</sup>Technical University “Gh. Asachi”, Iasi, Romania, e-mail: lgoras@zeta.etc.tuiasi.ro

<sup>2</sup>Technical University “Gh. Asachi”, Iasi, Romania, e-mail: t-teodor@zeta.etc.tuiasi.ro

**ABSTRACT** – Several new boundary conditions are studied for 2D CNN’s. Spatial eigenvectors and eigenvalues allowing the use of the differential equations decoupling are presented and computer simulations are given.

## 1. Introduction

Recent investigations [1-4] showed that, in certain conditions, CNNs based on second order cells produce patterns due to a reaction-diffusion mechanism similar to that proposed by Turing [5] to model morphogenesis.

For piece-wise non-linear characteristics of the cell resistors the first part of the transient towards a pattern (a stable equilibrium point [6]) certain predictions of the final pattern using the mode decoupling technique described in [3] are possible. Even though the theory the predictions are based on is linear the power of the decoupling technique is surprisingly good. Experimental results showed that such predictions are more reliable in the 1D case. In 2D case the results obtained using the decoupling technique are better when few modes fall inside the dispersion curve i.e. are unstable. As it is well known, boundary conditions may influence more or less the final pattern. In this communication, 2D eigenvectors and eigenvalues corresponding to a large class of boundary conditions are given and simulation results are presented.

## 2. Eigenvectors and Eigenvalues

Beside the classical ring and zero-flux, eight new BC have been presented in [7] for the 1D case. Even though other boundary conditions can be invented as well, their main feature is that analytic expressions for the eigenvectors and the corresponding eigenvalues have been found, allowing the use of the decoupling technique [3] to predict the final pattern. It became apparent that changing the boundary conditions, a certain control of the final pattern may be introduced, especially in the case of small arrays. Extensions to the 2D case is even more interesting due to the high number of possible combinations for the four sides of the array. Indeed, each combination of the 1D boundaries for each side of the array is possible. The boundary conditions in the 2D case will be ring, zero-flux, anti-zero- flux, quasi-zero-flux, zero, and combinations of the above on various sides of the array.

Denoting by  $k_m$ ,  $k_n$  and  $k_{mn}$  the spatial eigenvalue for the 1D respectively 2D cases and by  $\phi_M$ ,  $\phi_N$  and  $\phi_{MN}(m,n;i,j)$  the corresponding eigenfunctions, the following relationships are satisfied:

$$k_{mn}^2 = k_m^2 + k_n^2 \quad (1)$$

$$\phi_{MN}(m,n;i,j) = \phi_M(m,i)\phi_N(n,j)$$

where M and N are the two dimensions of the array and the spatial modes have been numbered from 0 to N-1 and M-1.

From the above relations it is apparent that, for a given dispersion curve corresponding to a particular choice of the cell and diffusion parameters, the number and the position of the unstable modes can be controlled by using various combinations of boundary conditions. Compared to the one-dimensional case, the number of possibilities is obviously much greater and the controlling method is more efficient in the case of small dimensional arrays.

In the table below we give examples of the eigenvectors and eigenvalues for several boundary conditions (same for the u and v “layer”).

	Boundary conditions	Eigenvectors	Eigenvalues
Anti-zero-flux on all boundaries	$u(-1,j)=-u(0,j)$ $u(M,j)=-u(M-1,j)$ $u(i,-1)=-u(i,0)$ $u(i,M)=-u(i,N-1,j)$ analogous for v	$\sin \frac{(m+1)(2i+1)\pi}{2M} \cdot \sin \frac{(n+1)(2j+1)\pi}{2N}$	$4\left(\sin^2 \frac{(m+1)\pi}{2M} + \sin^2 \frac{(n+1)\pi}{2N}\right)$

Zero on all boundaries	$u(-1,j)=0$ $u(M,j)=0$ $u(i,-1)=0$ $u(i,N)=0$ analogous for v	$\sin \frac{(m+1)(i+1)\pi}{M+1} \sin \frac{(n+1)(j+1)\pi}{N+1}$	$4\left(\sin^2 \frac{(m+1)\pi}{2(M+1)} + \sin^2 \frac{(n+1)\pi}{2(N+1)}\right)$
Quasi-zero-flux on all boundaries	$u(-1,j)=u(1,j)$ $u(M,j)=u(M-2,j)$ $u(i,-1)=u(i,1)$ $u(i,N)=u(i,N-2)$ analogous for v	$\cos \frac{mi\pi}{M-1} \cos \frac{nj\pi}{N-1}$	$4\left(\sin^2 \frac{m\pi}{2(M-1)} + \sin^2 \frac{n\pi}{2(N-1)}\right)$
Quasizero-flux-quasizero-flux zero-zero	$u(i,-1)=u(i,1)$ $u(i,N)=u(i,N-2)$ $v(i,-1)=v(i,1)$ $v(i,N)=v(i,N-2)$ $u(-1,j)=0$ $u(M,j)=0$ $v(-1,j)=0$ $v(M,j)=0$	$\cos \frac{mi\pi}{M-1} \sin \frac{(n+1)(i+1)\pi}{N+1}$	$4\left(\sin^2 \frac{m\pi}{2(M-1)} + \sin^2 \frac{(n+1)\pi}{2(N+1)}\right)$
Zero-zero-flux: antizero-flux-quasi-zero-flux	$u(i,-1)=0$ $v(i,-1)=0$ $u(i,N)=u(i,N-1)$ $v(i,N)=v(i,N-1)$ $u(-1,j)=-u(0,j)$ $v(-1,j)=-v(0,j)$ $u(M,j)=u(M-2,j)$ $v(M,j)=v(M-2,j)$	$\sin \frac{(2m+1)(i+1)\pi}{2M+1} \sin \frac{(2n+1)(j+1)\pi}{2(N+1)}$	$4\left(\sin^2 \frac{(2m+1)\pi}{2(2M+1)} + \sin^2 \frac{(2n+1)\pi}{2(2N+1)}\right)$

Table 1: Eigenvectors and their corresponding spatial eigenvalues

### 3. Computer simulation results

#### 3.1 Eigenvectors and eigenvalues

In the following, several simulations for various boundary and initial conditions are given. The parameters of the array and cells (Fig.1) are:  $M=N=5$ ,  $G_1=G_2=-1$ ,  $E_2=-E_1=1$ ,  $f_u=-(G+G_0)=0.4$ ,  $f_v=G/R=1.0$ ,  $g_u=C_u(G-g)/C_v=-0.25$ ,  $g_v=-C_u G/v=-0.5$ ,  $\gamma=1/C_u=15$ ,  $D_u=G_u/C_u=1.0$ ,  $D_v=G_v/C_v=3.8$  and  $D_v=3.3$  respectively ( $G_u$  and  $G_v$  are the conductances values of the two resistive grids). The dispersion curves for the two cases ( $D_v=3.8$  and  $D_v=3.3$ ) are characterized by peak at 1.77415,  $k_1^2=0.968037$ ,  $k_2^2=3.05828$ ,  $D_{\text{crit}}=3.27254$ ,  $k_{\text{crit}}=1.8541$  and peak at 1.84915,  $k_1^2=1.61056$ ,  $k_2^2=2.11672$  respectively. The property that  $D_v$  roughly moves vertically the dispersion curve is apparent from the fact that the band of unstable modes is significantly narrower in the second case.

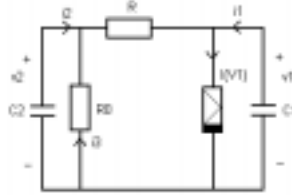


Figure 1: The cell

In the tables below the unstable modes and corresponding real parts of the temporal eigenvalues for  $D_v=3.8$  and  $D_v=3.3$  respectively and various types of boundary conditions are given:

$D_v=3.8$	Azf-Azf: Azf-Azf	Z-Z:Z-Z	Qzf-Qzf: Qzf-Qzf	Qzf-Qzf: Z-Z	Z-Zf: Azf-Qzf
m=0, n=1	$\text{Re}(\lambda)=0.378$	$\text{Re}(\lambda)=0.260$	-----	$\text{Re}(\lambda)=0.039$	$\text{Re}(\lambda)=0.124$
m=0, n=2	$\text{Re}(\lambda)=0.028$	$\text{Re}(\lambda)=0.307$	$\text{Re}(\lambda)=0.362$	$\text{Re}(\lambda)=0.362$	$\text{Re}(\lambda)=0.261$
m=0, n=3	-----	-----	-----	$\text{Re}(\lambda)=0.028$	-----

m=1, n=0	Re( $\lambda$ )=0.378	Re( $\lambda$ )=0.260	-----	-----	-----
m=1, n=1	Re( $\lambda$ )=0.134	Re( $\lambda$ )=0.362	Re( $\lambda$ )=0.199	Re( $\lambda$ )=0.365	Re( $\lambda$ )=0.376
m=1, n=2	-----	Re( $\lambda$ )=0.028	Re( $\lambda$ )=0.205	Re( $\lambda$ )=0.206	Re( $\lambda$ )=0.010
m=2, n=0	Re( $\lambda$ )=0.028	Re( $\lambda$ )=0.307	Re( $\lambda$ )=0.362	Re( $\lambda$ )=0.307	Re( $\lambda$ )=0.377
m=2, n=1	-----	Re( $\lambda$ )=0.028	Re( $\lambda$ )=0.205	Re( $\lambda$ )=0.028	Re( $\lambda$ )=0.155
m=3, n=0	-----	-----	-----	-----	Re( $\lambda$ )=0.051

Table 2: Unstable modes for  $D_v=3.8$

$D_v=3.3$	Azf-Azf: Azf-Azf	Z-Z:Z-Z	Qzf-Qzf: Qzf-Qzf	Qzf-Qzf: Z-Z	Z-Zf: Azf-Qzf
m=0, n=1	Re( $\lambda$ )=0.019	-----	-----	-----	-----
m=1, n=0	Re( $\lambda$ )=0.019	-----	-----	-----	-----
m=1, n=1	-----	Re( $\lambda$ )=0.014	-----	-----	Re( $\lambda$ )=0.013
m=0, n=2	-----	-----	Re( $\lambda$ )=0.014	Re( $\lambda$ )=0.015	-----
m=2, n=0	-----	-----	Re( $\lambda$ )=0.014	-----	Re( $\lambda$ )=0.022

Table 3: Unstable modes for  $D_v=3.3$

We emphasize that the tables above contain the real parts of the unstable modes only. It is easy to see that, due to the decrease of the width of the unstable band with the decrease of  $D_v$ , the number of unstable modes in the second case is smaller.

### 3.2 Patterns

Three different types of initial conditions have been used:

- random with a maximum 0.01 amplitude;
- single mode deterministic with a maximum 0.01 amplitude;
- combinations (sum) of the above, having as deterministic part one component of 0.01 and as random a 0.01 percent from the maximum amplitude of deterministic one.

In the first set of simulations  $D_v=3.8$  and random generated initial conditions and have been used. The results for various types of boundary conditions are presented in Figures 2-6. Even though, due to the non-linearity of the cells, the final pattern is not “pure”, the winner-modes are generally those which have the greatest real part for the temporal eigenvalue. However, as the spectral composition of the computer-generated noise is not constant, exceptions appear. This is the case of the results presented in Figures 5 and 6 when the modes m=1, n=1 respectively m=2, n=0 were expected and modes m=2, n=1 respectively m=1, n=1 were obtained.

The results presented in Figures 7-12 have been obtained with deterministic initial conditions for two values for parameters of  $D_v$ , in order to reflect the possibility of controlling the appearance of a pattern by using the boundary conditions. In Figures 7 and 12 the modes m=1 and n=1 for both values of  $D_v$  for the azf-azf:azf-azf boundary conditions have been used as initial conditions. From the two tables it is apparent that, in the case of  $D_v=3.3$ , no pattern should appear as the initialized mode was not in the band of unstable modes. Similar simulations have been done for the cases z-z:z-z, qzf-qzf:qzf-qzf, qzf-qzf:z-z and z-zf:azf-qzf boundaries, with modes (m=1, n=0), (m=1, n=2), (m=1, n=1) and (m=3, n=0) respectively. For  $D_v=3.8$ , the patterns were those predicted by the linear theory while for  $D_v=3.3$ , again according to linear theory predictions, there were no patterns as the initial conditions modes were not in the band of unstable modes (Fig. 12).

The results of the last set of simulations have been obtained using a sum between deterministic and random initial conditions for the case  $D_v=3.3$ . They are presented in Figures 13-17. We used the same deterministic components (with an amplitude of 0.01) as like for the simulations presented in Figure 12 and in addition, a level of 0.01% pseudo-random noise (generated with random() in C). The patterns corresponding to deterministic mode will not develop but generally, patterns obtained in Figures 2-6 will appear. An exception for qzf-qzf:z-z boundary appears, but, due to the fact that there is a single mode in the band of instability for  $D_v=3.3$ , a “clean<sup>1</sup>” pattern occurs. For the pseudo-random generated IC’s in  $D_v=3.8$ ’s case, there was more than

<sup>1</sup> We mean by “clean” a pattern whose spectrum has only one mode

one mode in the band of instability (with similar real parts) and derived from that, the pattern obtained was not a “clean” pattern.

#### **4. Concluding remarks**

Several new types of boundary conditions including analytical expressions for eigenvectors and eigenvalues have been given for the case of 2D Turing patterns producing CNN's. Computational results confirm the validity of theoretical results and the possibility of controlling patterns by means of choosing appropriate boundary conditions.

#### **References**

- [1] L. O. Chua, M. Hasler, G. S. Moschytz and J. Neiryneck, “Autonomous Cellular Neural Networks: A Unified Paradigm for Pattern Formation and Active Wave Propagation, IEEE Trans. Circuits Syst, vol. 42, pp. 559-577, October 1995.
- [2] L. Goraş, L. O. Chua, D.M.W. Leenaerts, “Turing Patterns in CNN's - Part I: Once Over Lightly”, IEEE Trans. Circuits Syst, vol. 42, pp. 602-611, October 1995.
- [3] L. Goraş, L. O. Chua, “Turing Patterns in CNN's - Part II: Equations and Behaviors”, IEEE Trans. Circuits Syst, vol. 42, pp. 612-626, October 1995.
- [4] L. Goraş, L. O. Chua, L. Pivka, “Turing Patterns in CNN's - Part III: Computer Simulation Results”, IEEE Trans. Circuits Syst, vol. 42, pp. 627-636, October 1995.
- [5] A. M. Turing, “The Chemical Basis of Morphogenesis”, Phil. Trans. Roy. Soc. Lond. B 237, pp. 37-72, October 1952.
- [6] T. Teodorescu, L. Goraş, “On the Dynamics of Turing Pattern Formation in 1D CNN's”, Proceedings SCS97, Iasi, pp. 109-112, October 1997.
- [7] L. Goraş, L. O. Chua, “On the Influence of CNN Boundary Conditions in Turing Pattern Formation”, Proceedings ECCTD97, Budapest, pp. 383-388, September 1997.

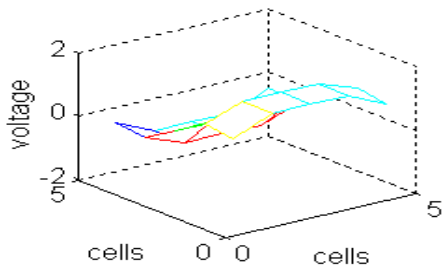


Figure 2:  $azf-azf:azf-azf$ ,  $Dv=3.8$ ,  $u$  side

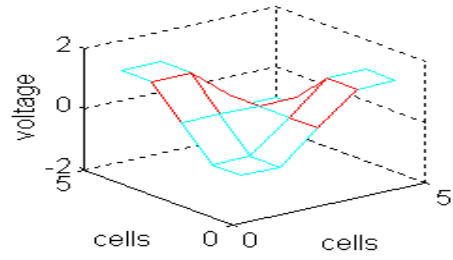


Figure 3:  $z-z:z-z$ ,  $Dv=3.8$ ,  $u$  side

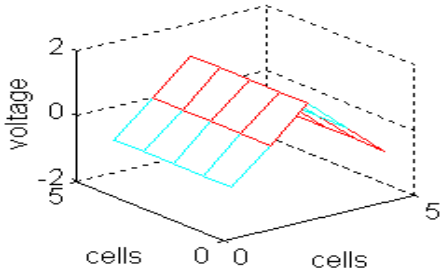


Figure 4:  $qzf-qzf:qzf-qzf$ ,  $Dv=3.8$ ,  $u$  side

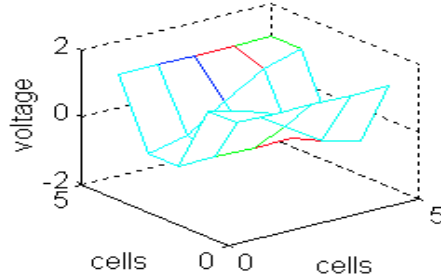


Figure 5:  $qzf-qzf:z-z$ ,  $Dv=3.8$ ,  $u$  side

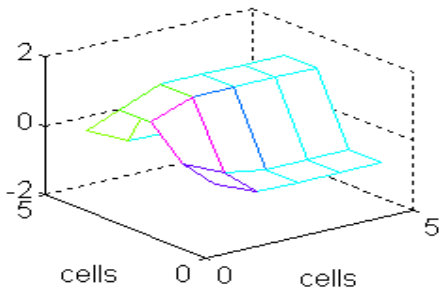


Figure 6:  $z-zf:azf-qzf$ ,  $Dv=3.8$ ,  $u$  side

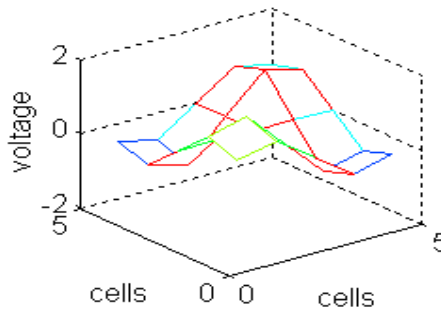


Figure 7:  $azf-azf:azf-azf$ ,  $Dv=3.8$ ,  $Det(1,1)$ ,  $u$  side

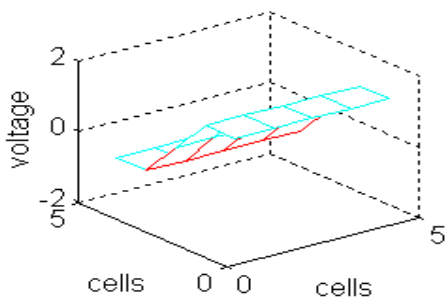


Figure 8:  $z-z:z-z$ ,  $Dv=3.8$ ,  $Det(1,0)$ ,  $u$  side,

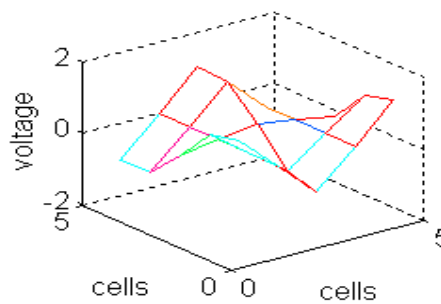


Figure 9:  $qzf-qzf:qzf-qzf$ ,  $Dv=3.8$ ,  $Det(1,2)$ ,  $u$  side

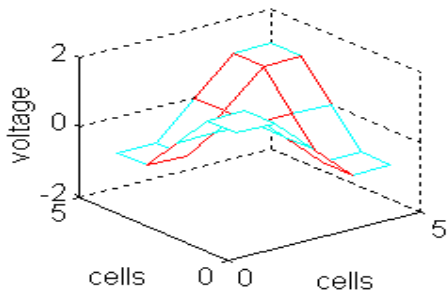


Figure 10:  $qzf-qzf:z-z$ ,  $Dv=3.8$ ,  $Det(1,1)$ ,  $u$  side

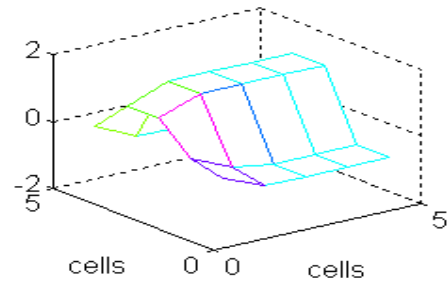


Figure 11:  $z-zf:azf-qzf$ ,  $Dv=3.8$ ,  $Det(3,0)$ ,  $u$  side

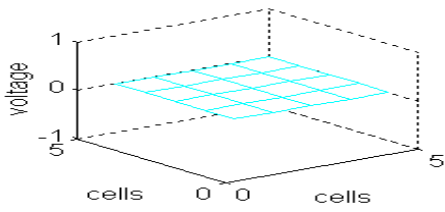


Figure 12:  $azf-azf:azf-azf$ ,  $Dv=3.3$ ,  $Det(1,1)$ ;  
 $z-z:z-z$ ,  $Dv=3.3$ ,  $Det(1,0)$ ;  
 $qzf-qzf:qzf-qzf$ ,  $Dv=3.3$ ,  $Det(1,2)$ ;  
 $qzf-qzf:z-z$ ,  $Dv=3.3$ ,  $Det(1,1)$ ;  
 $z-zf:azf-qzf$ ,  $Dv=3.3$ ,  $Det(3,0)$ ,  $u$  side

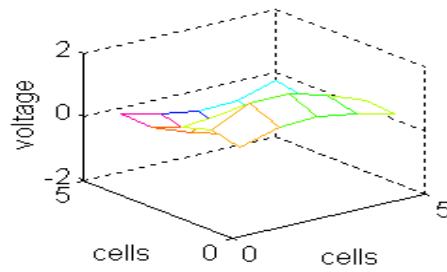


Figure 13:  $azf-azf:azf-azf$ ,  $Dv=3.3$ ,  $0.01\%rand+Det(1,1)$ ,  $u$  side

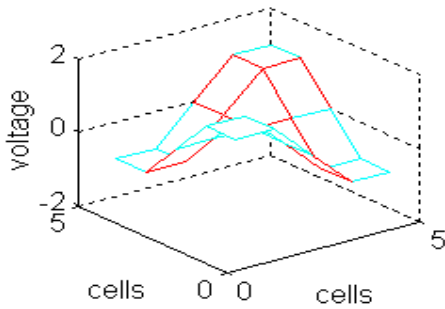


Figure 14:  $z-z:z-z$ ,  $Dv=3.3$ ,  $0.01\%rand+Det(1,0)$ ,  $u$  side

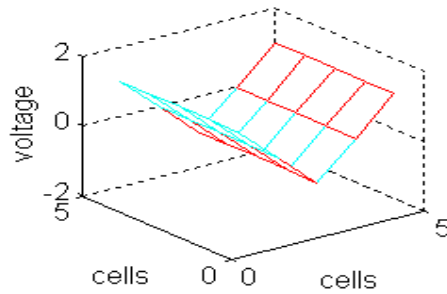


Figure 15:  $qzf-qzf:qzf-qzf$ ,  $Dv=3.3$ ,  $0.01\%rand+Det(1,2)$ ,  $u$  side

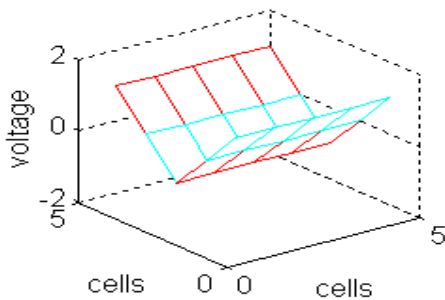


Figure 16:  $qzf-qzf:z-z$ ,  $Dv=3.3$ ,  $0.01\%rand+Det(1,1)$ ,  $u$  side

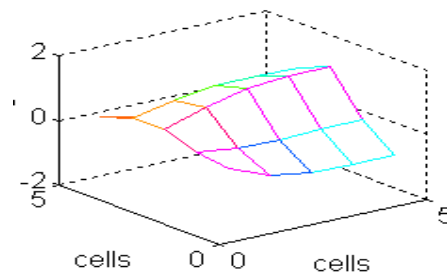


Figure 17:  $z-zf:azf-qzf$ ,  $Dv=3.3$ ,  $0.01\%rand+Det(3,0)$ ,  $u$  side